Available online at www.sciencedirect.com
ScienceDirect
Journal of Molecular Catalysis A: Chemical 260 (2006) 56–61
JOURNAL OF MOLECULAR CATALYSIS A: CHEMICAL
www.elsevier.com/locate/molcata

# Characterizations and photocatalytic activity of nanocrystalline $La_{1.5}Ln_{0.5}Ti_2O_7$ (Ln = Pr, Gd, Er) solid solutions prepared via a polymeric complex method

Zhaohui Li, Hun Xue, Xuxu Wang, Xianzhi Fu *

*Institute of Photocatalysis, Fuzhou University, Fuzhou 350002, PR China*

Received 10 June 2006; received in revised form 28 June 2006; accepted 29 June 2006
Available online 14 August 2006

**Abstract**

Nanocrystalline $La_{1.5}Ln_{0.5}Ti_2O_7$ (Ln = Pr, Gd, Er) solid solutions were prepared by a polymeric complex method. The samples were characterized by X-ray diffraction (XRD) analysis, transmission electron microscopy (TEM), UV–vis diffuse reflectance spectra (DRS), energy dispersive X-ray spectrum (EDS), thermogravimetric analyses (TGA) and differential thermal analyses (DTA). The photocatalytic activity of $La_{1.5}Ln_{0.5}Ti_2O_7$ (Ln = Pr, Gd, Er) was evaluated by the photocatalytic degradation of methyl orange (MO). $La_{1.5}Gd_{0.5}Ti_2O_7$ showed the best photocatalytic activity and it was supposed that the half-filled electronic configuration of $Gd^{3+}$ can promote charge transfer and enhance the photocatalytic activity. The difference in the photocatalytic activity observed for $La_{1.5}Ln_{0.5}Ti_2O_7$ (Ln = La, Pr, Gd, Er) can be related to the different Ln 4f shell.


*Keywords:* Solid solution; $La_2Ti_2O_7$; Photocatalytic; Polymeric complex method

## 1. Introduction

$La_2Ti_2O_7$ has a layered perovskite structure with a general formula of $A_2B_2O_7$ [1–7]. $La_2Ti_2O_7$ has been extensively studied as photocatalyst materials for water splitting [1–4,6,7], optical materials [8], ferroelectric device components [9,10] and so on. The crystal structure of $La_2Ti_2O_7$ (Fig. 1) indicates that $La_2Ti_2O_7$ is built of layers of distorted perovskite-like slabs running parallel to the (1 1 0) plane bounded to each other by interlayer $La^{3+}$ ions. The thickness of the slabs corresponds approximately to four corner-linked $TiO_6$ octahedral [6].

A layer-perovskite-structured metal oxide $A_2B_2O_7$ provides a good base material for chemical substitutions. Both A sites and B sites in $A_2B_2O_7$ can be substituted by diverse component ions to form stable solid solutions. The formations of stable solid solutions via partly substitutions of Ti sites by $Cr^{3+}$, $Fe^{3+}$ [4] and La sites by $Pr^{3+}$, $Nd^{3+}$ in $La_2Ti_2O_7$ have been reported by Lee et al. [1]. It was reported that the band structure and the photocatalytic activity for water splitting of the resultant solid solutions could be greatly influenced by the substituted Ln ions due to their different 4f shell.

Although $La_2Ti_2O_7$-based solid solutions have been investigated as efficient photocatalysts for water splitting, the applications of such materials in the photocatalytic degradations of organic pollutants have seldom been reported so far [5]. It would be interesting to explore the feasibility of the applications of $La_2Ti_2O_7$ based materials in the photocatalytic decomposition of organic pollutants and how the substitutions would affect the photocatalytic activities of these solid solutions. Since multi-component oxides prepared by the polymeric complex method have been reported to exhibit much higher photocatalytic activities than those prepared by traditional solid-state reactions [6], in this paper we prepared Ln ions (Ln = Pr, Gd, Er) substituted $La_2Ti_2O_7$ solid solutions via a polymeric complex method. The structures and photophysical properties of the prepared solid solutions were characterized and their photocatalytic activity was evaluated by the degradation of the typical dye methyl orange (MO). The comparative studies of these $La_2Ti_2O_7$ based materials showed that their structures and photophysical properties can be tuned by Ln ions substitutions. Highly enhanced photocatalytic activity was observed on $Gd^{3+}$-substituted $La_2Ti_2O_7$, whereas $Nd^{3+}$ or $Pr^{3+}$ substitutions only

* Corresponding author. Fax: +86 591 83738608.
*E-mail address:* xzfu@fzu.edu.cn (X. Fu).

1381-1169/$ – see front matter © 2006 Elsevier B.V. All rights reserved.
doi:10.1016/j.molcata.2006.06.056

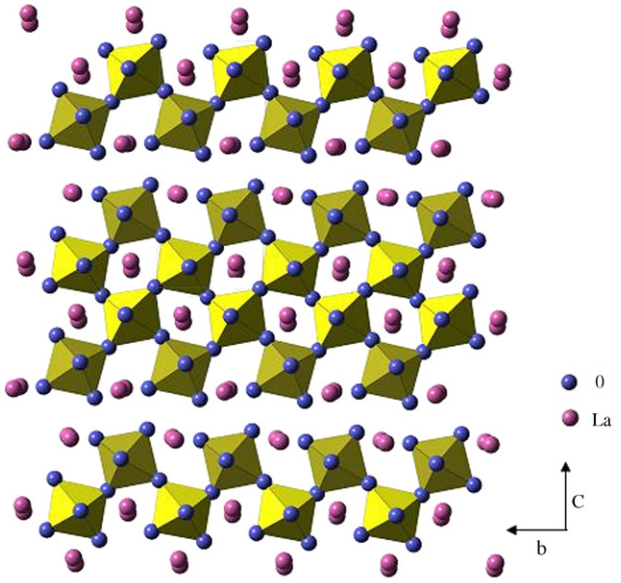


Fig. 1. Schematic diagram of $La_2Ti_2O_7$.

lead to the decreased photocatalytic activity. The difference in the photocatalytic activity can be related to the different Ln 4f shell.

## 2. Experimental

### 2.1. Synthesis

Scheme 1 showed a flowchart of the synthesis procedure for $La_{1.5}Ln_{0.5}Ti_2O_7$ (Ln = Pr, Gd, Er) solid solutions via a polymeric complex method. Tetra-*n*-butyl titanate, $La(NO_3)_3{\cdot}6H_2O$, $Er(NO_3)_3{\cdot}5H_2O$, $Pr(NO_3)_3{\cdot}6H_2O$, $Gd(NO_3)_3{\cdot}6H_2O$ and citric acid were used as the starting materials. For a typical experiment, an amount of 2 mmol of tetra-*n*-butyl titanate was first dissolved into 80 mL of ethylene glycol, and subsequently 4 mmol of citric acid was added to this solution. After complete dissolution, 1.5 mol of $La(NO_3)_3{\cdot}6H_2O$ and 0.5 mol of $Ln(NO_3)_3{\cdot}XH_2O$ (Ln = Pr, Gd, Er) were added. The mixture was stirred magnetically for several hours at 70 °C until it became a transparent clear solution. The solution obtained was heated at 130 °C with stirring for several hours to form a polymeric gel. The polymeric gel was dried at 150 °C in baking oven to form precursor. The precursors thus obtained were calcinated at 800 °C for 5 h to obtain $La_{1.5}Ln_{0.5}Ti_2O_7$ (Ln = Pr, Gd, Er) solid solutions.

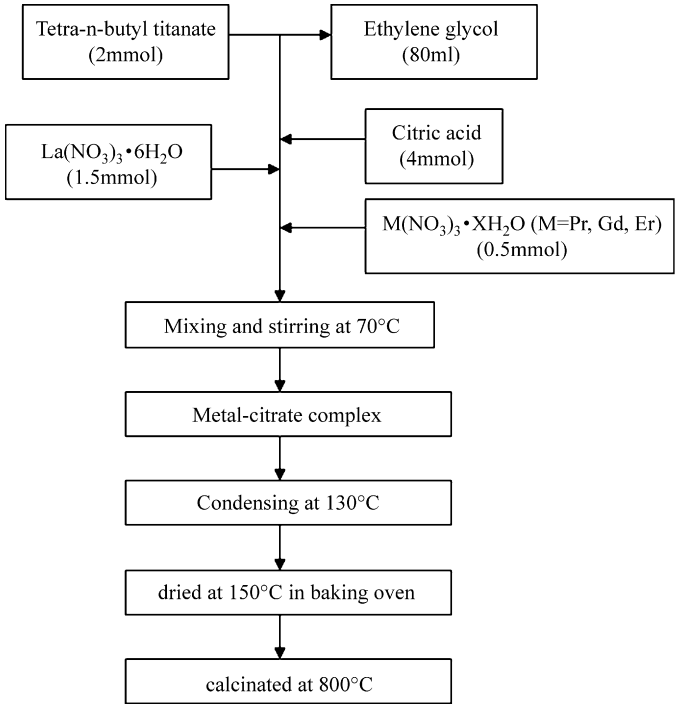


Scheme 1. Flowchart of syntheses of $La_{1.5}Ln_{0.5}Ti_2O_7$ (Ln = Pr, Gd, Er) solid solutions via a polymeric complex method.

### 2.2. Characterizations

X-ray diffraction (XRD) patterns were collected on a Bruker D8 Advance X-ray diffractometer with Cu Kα radiation. The accelerating voltage and the applied current were 40 kV and 40 mA, respectively. Data were recorded at a scanning rate of 0.1° $2\theta\,s^{-1}$ in the $2\theta$ range 10–60°. It was used to identify the phases presented and their crystallite sizes. The crystallite size was calculated from X-ray line broadening analysis by the Scherer equation: $D = 0.89\lambda/\beta\cos\theta$, where $D$ is the crystal size in nm, λ the Cu Kα wavelength (0.15406 nm), $\beta$ the half-width of the peak in radians, and $\theta$ is the corresponding diffraction angle. UV–vis absorption spectra of the powders were obtained for the dry-pressed disk samples using a UV–vis spectrophotometer (Cary 500 Scan Spectrophotometers, Varian, USA). $BaSO_4$ was used as a reflectance standard in the UV–vis diffuse reflectance experiment. Thermogravimetric analyses (TGA) and differential thermal analyses (DTA) were performed on a TG-DTA Netzsch Sta 449C thermal analysis instrument. Measurement was taken with a heating rate of 10 °C/min from 50 to 800 °C. The transmission electron microscopy (TEM) and high-resolution transmission electron microscopy (HRTEM) images were measured by JEOL model JEM 2010 EX instrument at the accelerating voltage of 200 kV. The powder particles were supported on a carbon film coated on a 3 mm diameter fine-mesh copper grid. A suspension in ethanol was sonicated, and a drop was dripped on the support film.

### 2.3. Photocatalytic activity measurements

Photocatalytic reactions were performed in a quartz tube with 4.7 cm inner diameter and 16.5 cm length. Four 4 W UV lamps with a wavelength centered at 254 nm (Philips, TUV 4W/G4 T5) were used as illuminating source. 150 mg of powdered photocatalysts were suspended in 150 mL of MO aqueous solution ($1 \times 10^{-5}$ mol/L) and stirred for 1 h before irradiation to ensure the reach of the adsorption/desorption equilibrium. A 4 mL aliquot was taken at 30 min intervals during the experiment and centrifuged (TDL-5-A). The resulting clear liquor was analyzed on a Varian UV–vis–NIR spectrophotometer (model: Cary-500). The percentage of degradation is reported as $C/C_0$. $C$ is the absorption of methyl orange at each irradiated time inter-

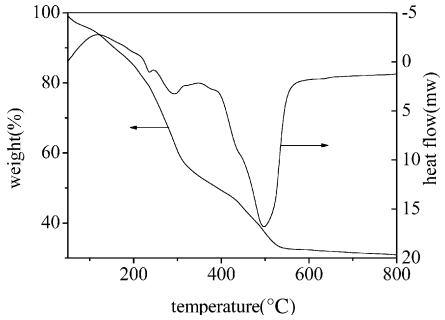


Fig. 2. TGA and DTA curves for $La_{1.5}Gd_{0.5}Ti_2O_7$ precursor.

val of the main peak of the absorption spectrum at wavelength 464 nm. $C_0$ is the absorption of the starting concentration when adsorption/desorption equilibrium was achieved.

## 3. Results and discussion

### 3.1. TG and DTA studies

TGA and DTA were performed on the as-synthesized $La_{1.5}Gd_{0.5}Ti_2O_7$ precursor to determine the calcination temperature. The TGA curve showed two continuous weight losses in the range of 50–350 °C and 350–550 °C (Fig. 2). The first weight loss could be due to the dehydration and the partly decomposition of the citrate. The second weight loss could be ascribed to the decomposition of the residual organics involved in the intermediate product. DTA results showed four features. The endothermic peak at ca. 120 °C might be from the removal of the adsorbed waters. Two exothermic peaks in the region of 230–350 °C were attributed to the partly decomposition of the organics. The largest exothermic peak around 510 °C could be due to the burn out of the residual organics. The thermoanalysis results indicated that the totally removal of the organics can only happened above 550 °C.

The XRD patterns of $La_{1.5}Gd_{0.5}Ti_2O_7$ precursor calcinated in air at various temperatures as shown in Fig. 3 supported the thermoanalysis results. Crystalline $La_{1.5}Gd_{0.5}Ti_2O7$ can only be obtained after calcinated at temperature higher than 600 °C (Fig. 3). To obtain better crystalline samples, 800 °C was chosen in the synthesizing of $La_{1.5}Ln_{0.5}Ti_2O_7$ (Ln = Pr, Gd, Er) solid solutions.

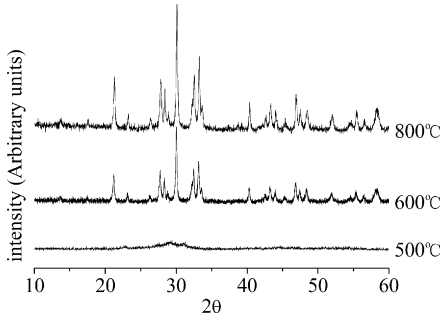


Fig. 3. XRD patterns of products obtained by calcinating $La_{1.5}Gd_{0.5}Ti_2O_7$ precursor in air for 5 h at (a) 500 °C; (b) 600 °C; (c) 800 °C.

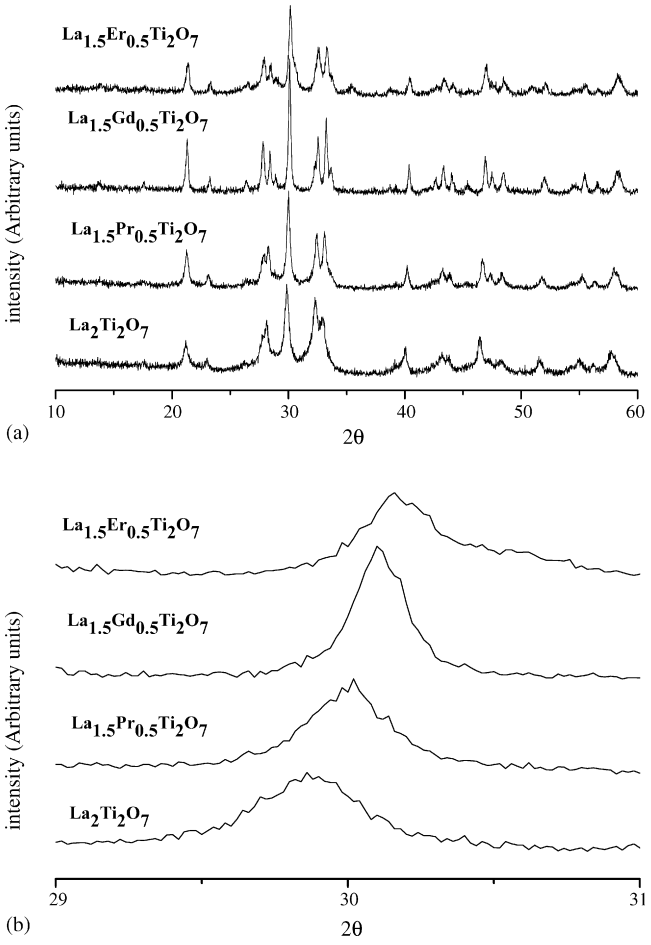


Fig. 4. XRD patterns of $La_{1.5}Ln_{0.5}Ti_2O_7$ (Ln = La, Pr, Gd, Er).

### 3.2. XRD analyses

Fig. 4a showed the XRD patterns of $La_2Ti_2O_7$ and $La_{1.5}Ln_{0.5}Ti_2O_7$ (Ln = Pr, Gd, Er) solid solutions prepared via the polymeric complex method. All the peaks match well with the characteristic reflections of $La_2Ti_2O_7$ (JCPDS card 28-517) and literature results [1,6,11]. All the peaks could be ascribed to the monoclinic $La_2Ti_2O_7$ and no impurity phases were detected. An expanded view of the peak corresponding to (2 1 2) plane was shown in Fig. 4b. The lattice constants of $La_2Ti_2O_7$ and $La_{1.5}Ln_{0.5}Ti_2O_7$ (Ln = Pr, Gd, Er) solid solutions calculated from the *d*-spacing of the X-ray diffraction pattern were summarized in Table 1. The *d*-spacing of the (2 1 2) plane and the unit-cell volumes both followed the order of $La_2Ti_2O_7 > La_{1.5}Pr_{0.5}Ti_2O_7 > La_{1.5}Gd_{0.5}Ti_2O_7 > La_{1.5}Er_{0.5}Ti_2O_7$. This result is reasonable considering the ionic radius of eight-coordinated $Ln^{3+}$ (1.16, 1.13, 1.05, 1.00 Å for $La^{3+}$, $Pr^{3+}$, $Gd^{3+}$, $Er^{3+}$, respectively) [12].

### 3.3. UV–vis diffuse reflectance spectra

Fig. 5 showed the UV–vis diffuse reflectance spectra of $La_2Ti_2O_7$ and $La_{1.5}Ln_{0.5}Ti_2O_7$ (Ln = Pr, Gd, Er) solid solutions. The band-gap transitions showed red shifts when Pr, Er

Table 1
Lattice constants of $La_{1.5}Ln_{0.5}Ti_2O_7$ (Ln = La, Pr, Gd, Er)

| Lattice parameter | $La_2Ti_2O_7$ | $La_{1.5}Pr_{0.5}Ti_2O_7$ | $La_{1.5}Gd_{0.5}Ti_2O_7$ | $La_{1.5}Er_{0.5}Ti_2O_7$ |
|---|---|---|---|---|
| *d*-Spacing of (2 1 2) plane (Å) | 2.991 | 2.987 | 2.978 | 2.974 |
| *a* (Å) | 13.011 | 13.006 | 12.945 | 12.928 |
| *b* (Å) | 5.546 | 5.535 | 5.495 | 5.489 |
| *c* (Å) | 7.812 | 7.784 | 7.744 | 7.718 |
| *V* (Å$^3$) | 557.31 | 554.00 | 544.60 | 541.47 |

or Gd substituted for La in $La_2Ti_2O_7$. The color of $La_2Ti_2O_7$, $La_{1.5}Pr_{0.5}Ti_2O_7$, $La_{1.5}Er_{0.5}Ti_2O_7$ and $La_{1.5}Gd_{0.5}Ti_2O_7$ were white, light green, pink and white, respectively. The visible-light absorption observed for $La_{1.5}Pr_{0.5}Ti_2O_7$ and $La_{1.5}Er_{0.5}Ti_2O_7$ could be ascribed to the internal transitions in a partially filled Ln 4f shell.

### 3.4. TEM, HRTEM and EDS

The TEM image of $La_{1.5}Er_{0.5}Ti_2O_7$ (Fig. 6a) showed that the average value of the nanocrystalline $La_{1.5}Er_{0.5}Ti_2O_7$ was around 35 nm, which was consistent with the value obtained from XRD patterns using the Scherrer formula. Some aggregations among the particles could be observed. The HRTEM images (Fig. 6b and c) showed clear lattice fringes. The fringes of $d = 0.27$ and 0.29 nm matched that of the (4 0 0) and (2 1 2) crystallographic planes of $La_{1.5}Er_{0.5}Ti_2O_7$. The EDS pattern showed that the samples contain only La, Ti, Er and O elements. The atomic ratio of La, Er and Ti was about 1.5:0.5:2, in agreement with the expected stoichiometry.

### 3.5. Photocatalytic activity

Although $La_{1.5}Er_{0.5}Ti_2O_7$ and $La_{1.5}Pr_{0.5}Ti_2O_7$ are visible-light responsive, they did not show any photocatalytic activities under visible light illumination. So the photocatalytic activities of the as-prepared samples were evaluated by measuring the degradation of MO under UV illumination. Temporal changes in the concentration of MO were monitored by examining the variations in maximal absorption in UV–vis spectra at 464 nm. Fig. 7 showed the results of the degradation of MO in the presence of different samples. It was found that the order of the photocatalytic activities was as following: $La_{1.5}Gd_{0.5}Ti_2O_7 > La_2Ti_2O_7 > La_{1.5}Er_{0.5}Ti_2O_7 > La_{1.5}Pr_{0.5}Ti_2O_7$.

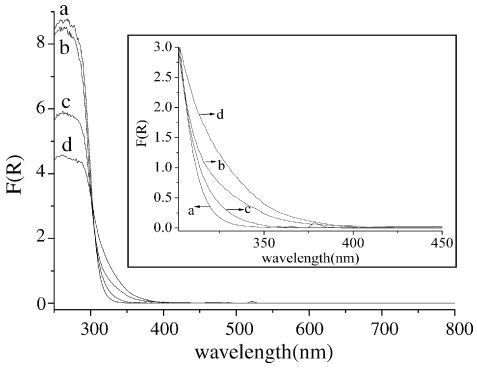


Fig. 5. UV–vis diffuse reflectance spectra of $La_{1.5}Ln_{0.5}Ti_2O_7$: (a) $La_2Ti_2O_7$; (b) $La_{1.5}Pr_{0.5}Ti_2O_7$; (c) $La_{1.5}Er_{0.5}Ti_2O_7$; (d) $La_{1.5}Gd_{0.5}Ti_2O_7$.

Since all the solid solutions have the same layered perovskite-type structure, the reason why $La_{1.5}Gd_{0.5}Ti_2O_7$ showed the highest reactivity may be related to the special electronic configuration of $Gd^{3+}$. $Gd^{3+}$ is different from the other rare earth ions in that it has a half filled f shell. The systematic studies by Choi et al. had shown that $Fe^{3+}$, $Ru^{3+}$ and $Os^{3+}$ (all have half-filled electronic configuration) doped $TiO_2$ showed the highest photocatalytic activities [13]. Xu et al. also reported that among all the rare earth ions doped $TiO_2$, $Gd^{3+}$-doped $TiO_2$ showed the highest photocatalytic activity towards the photodegradation of nitrite [14]. According to Xu et al., the half-filled configuration of the metal ion is more stable and when such a configuration is destroyed, it has a strong tendency to return to the original stable state. This particular characteristic of the dopant ion with the half-filled electronic configuration can promote the charge transfer and efficiently separate the electron–hole pairs by shallowly trapping electrons. Although other metal ions can also trap the photo-exicted electrons, the detrapping is more difficult on these metal ions. So $La_{1.5}Gd_{0.5}Ti_2O_7$ has higher efficiency in the separation and transfer of charge carriers and thus shows higher reactivity than other rare-earth $La_{1.5}Ln_{0.5}Ti_2O_7$ (Ln = La, Er and Pr).

The photocatalytic activities of the other three complexes followed the order of $La_2Ti_2O_7 > La_{1.5}Er_{0.5}Ti_2O_7 > La_{1.5}Pr_{0.5}Ti_2O_7$. Lee et al. have reported that the photocatalytic activity for water splitting on $La_2Ti_2O_7$ was superior to that of $LaPrTi_2O_7$ [1]. According to his calculations on the band structure of these two complexes, he concluded that the conduction band of $La_2Ti_2O_7$ consisted mainly of broad Ti 3d and sharp La 4f orbital and when La was substituted with Pr, the band gap would become smaller due to a lower 4f level of Pr compared to that of La [15,16]. A smaller band gap is disadvantageous for the suppression of the recombination of electron–hole pairs and leads to a decrease in the photocatalytic activity for water splitting. In our experiment, although the band structures of $La_{1.5}Er_{0.5}Ti_2O_7$ and $La_{1.5}Pr_{0.5}Ti_2O_7$ were not calculated, the DRS results suggested that when La was substituted with Pr or Er, the band gap transition showed red-shift and thus indicated a smaller band gap in $La_{1.5}Er_{0.5}Ti_2O_7$ and $La_{1.5}Pr_{0.5}Ti_2O_7$ compared to $La_2Ti_2O_7$. So a higher photocatalytic activity observed for $La_2Ti_2O_7$ can be attributed to a larger band gap.

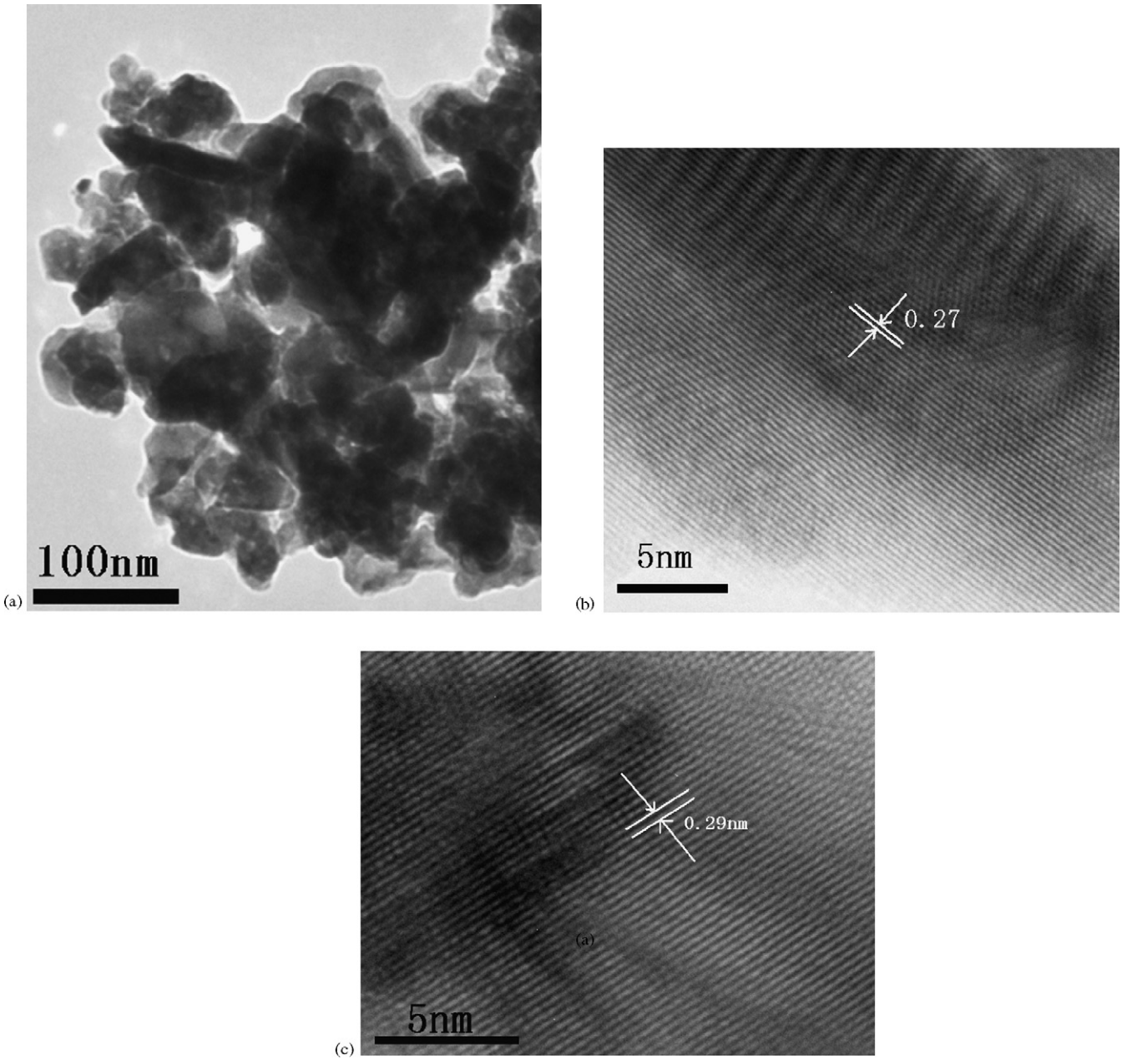


Fig. 6. TEM and HRTEM images of $La_{1.5}Er_{0.5}Ti_2O_7$.

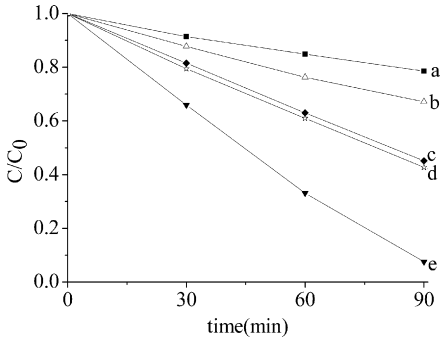


Fig. 7. Photocatalytic degradation of MO under UV illumination (λ = 254 nm): (a) photolysis; (b) $La_{1.5}Pr_{0.5}Ti_2O_7$; (c) $La_{1.5}Er_{0.5}Ti_2O_7$; (d) $La_2Ti_2O_7$; (e) $La_{1.5}Gd_{0.5}Ti_2O_7$.

## 4. Conclusions

Nanocrystalline $La_2Ti_2O_7$ and $La_{1.5}Ln_{0.5}Ti_2O_7$ (Ln = Pr, Gd, Er) solid solutions were successfully synthesized by a polymeric complex method. The characterization results showed that $Ln^{3+}$ (Pr, Gd, Er) were substituted for La sites in the $La_2Ti_2O_7$ lattice. $La_{1.5}Gd_{0.5}Ti_2O_7$ showed the best photocatalytic activity in the decomposition of MO and it was supposed that the half-filled electronic configuration of $Gd^{3+}$ can promote charge transfer and enhance the photocatalytic activity. Different photocatalytic activity observed for $La_{1.5}Ln_{0.5}Ti_2O_7$ (Ln = La, Pr, Gd, Er) can be related to the different Ln 4f shell.

## Acknowledgments

The work was supported by National Natural Science Foundation of China (20537010, 20573020, 20571015, 2004CCA07100), grants from Fujian Province (E0410009, 2003J011, 2005K003). Z. Li thanks program for New Century Excellent Talents in University and the Scientific Research Foundation for the Returned Overseas Chinese Scholars, State Education Ministry.

## References

[1] K.W. Hwang, J.S. Lee, W. Li, S.H. Oh, J. Phys. Chem. B 107 (2003) 4963.
[2] H.G. Kim, D.W. Hwang, J. Kim, Y.G. Kim, J.S. Lee, Chem. Commun. (1999) 1077.
[3] J. Kim, D.W. Hwang, H.G. Kim, S.W. Bae, S.M. Ji, J.S. Lee, Chem. Commun. (2002) 2488.
[4] D.W. Hwang, H.G. Kim, J.S. Lee, J. Kim, W. Li, S.H. Oh, J. Phys. Chem. B 109 (2005) 2093.
[5] D.W. Hwang, K.Y. Cha, J. Kim, G. Kim, S.W. Bae, J.S. Lee, Ind. Eng. Chem. Res. 42 (2003) 1184.
[6] H.G. Kim, K.W. Hwang, S.W. Bae, J.H. Jung, J.S. Lee, Catal. Lett. 91 (2003) 193.
[7] D.W. Hwang, H.G. Kim, J.S. Jang, S.W. Bae, S.M. Ji, J.S. Lee, Catal. Today 93 (2004) 845.
[8] P.T. Diallo, P. Boutinaud, R. Mahiou, J. Alloy Compd. 341 (2002) 139.
[9] Y.A. Titov, A.M. Sych, V.Y. Markiv, N.M. Belyavina, A.A. Kapshuk, V.P. Yaschuk, J. Alloys Compd. 316 (2001) 309.
[10] A.D. Li, Y.J. Wang, S. Huang, J.B. Cheng, D. Wu, N.B. Ming, J. Crystal Growth 268 (2004) 198.
[11] M.M. Milanova, M. Kakihana, M. Arima, M. Yashima, M. Yoshimura, J. Alloy Compd. 242 (1996) 6.
[12] J.A. Dean, Lange's Handbook of Chemistry, 15th ed., McGraw-Hill, 1999.
[13] W. Choi, A. Termin, M.R. Hoffmann, J. Phys. Chem. 98 (1994) 13669.
[14] A.W. Xu, Y. Gao, H.Q. Liu, J. Catal. 207 (2002) 151.
[15] M. Machida, S. Murakami, T. Kijima, S. Matsushima, M. Arai, J. Phys. Chem. B 105 (2001) 3189.
[16] M. Machida, J. Yabunaka, T. Kijima, S. Matsushima, M. Arai, Int. J. Inorg. Mater. 3 (2001) 545.